Supercond. Sci. Technol. **23** (2010) 014005 (7pp) doi:10.1088/0953-2048/23/1/014005

Enhanced flux pinning in MOCVD-YBCO films through Zr additions: systematic feasibility studies

T Aytug[1], M Paranthaman[1], E D Specht[1], Y Zhang[1], K Kim[1], Y L Zuev[1], C Cantoni[1], A Goyal[1], D K Christen[1], V A Maroni[2], Y Chen[3] and V Selvamanickam[3]

[1] Oak Ridge National Laboratory, Oak Ridge, TN 37831, USA
[2] Argonne National Laboratory, Argonne, IL 60439, USA
[3] SuperPower, Incorporated, 450 Duane Avenue, Schenectady, NY 12304, USA

E-mail: aytugt@ornl.gov

Received 17 May 2009, in final form 7 July 2009
Published 9 December 2009
Online at stacks.iop.org/SUST/23/014005

Abstract
Systematic effects of Zr additions on the structural and flux pinning properties of $YBa_2Cu_3O_{7-\delta}$ (YBCO) films deposited by metal–organic chemical vapor deposition (MOCVD) have been investigated. Detailed characterization, conducted by coordinated transport, x-ray diffraction, scanning and transmission electron microscopy analyses, and imaging Raman microscopy have revealed trends in the resulting property/performance correlations of these films with respect to varying mole percentages (mol%) of added Zr. For compositions $\leqslant$7.5 mol%, Zr additions lead to improved in-field critical current density, as well as extra correlated pinning along the *c*-axis direction of the YBCO films via the formation of columnar, self-assembled stacks of $BaZrO_3$ nanodots.

(Some figures in this article are in colour only in the electronic version)

1. Introduction

In order to realize the full potential of high temperature superconducting wires (HTS coated conductors) for various commercial electric-power equipment, the flux pinning properties of $REBa_2Cu_3O_{7-\delta}$ films (REBCO, RE = Y or a rare earth element) need to be improved in a controlled, reproducible and practical fashion [1–3]. In fact, these are the key requirements for scalable deposition approaches producing large-scale, long-length, continuous conductors. Improvements in pinning efficiency not only enhance the critical current density, J_c, under high magnetic fields, B, but also may help reduce the field dependent anisotropy in J_c for in-field orientations ranging from the *ab*-plane to the *c*-axis. The latter advancement is especially important for such power utility applications as motors, generators, and transmission lines, where HTS cables experience varying magnetic field strengths and directions. In recent years, the issue of improving the effective pinning of magnetic flux lines in HTS films has been successfully addressed by many groups through manipulation of defects in REBCO film matrix [3]. That is, through various methods of deposition-controlled nanostructural engineering, additional pinning centers of different sizes and morphologies, in addition to the existing naturally formed growth-induced defects, have been introduced into REBCO films. One particularly successful and heavily studied dopant is $BaZrO_3$ (BZO), first incorporated into the YBCO films, in the form of 5–100 nm size particles [4], by pulsed laser deposition (PLD). This was followed by the demonstration of strain-induced formation of columnar defects, comprising self-assembled nanodots and/or nanorods of BZO within the superconducting matrix [5–7]. Similar columnar defects were also observed by incorporation of yttria-stabilized zirconia (YSZ) in REBCO films [8]. The columnar defects have proven to be very effective for enhancing the pinning performance, especially for fields applied near the *c*-axis of the REBCO film. Creation of such columnar defects has recently been shown possible using the scalable and economically tenable technique of metal–organic chemical vapor deposition (MOCVD) [9].

 © 2010 IOP Publishing Ltd Printed in the UK

We present herein results of systematic studies of varying mole percentages (mol%) of Zr additions to MOCVD-YBCO precursors to understand the effects and trends in the structural properties and pinning performance of the resulting films. Through detailed property characterizations, we have correlated different levels of Zr content with microstructural as well as electrical transport properties of YBCO films.

2. Experimental details

A vertically aligned research-scale MOCVD apparatus, based on a liquid-state precursor delivery system, was used to deposit the YBCO films. The details of this SuperPower-based, custom-designed system have been described elsewhere [10]. Briefly, the organometallic tetramethyl heptanedionate (thd) complexes of individual liquid precursor solutions for Y, Ba, Cu and Zr were mixed together in an appropriate mole ratio (Y:Ba:Cu = 1.3:2:2.6), and then delivered at a controlled pumping rate to an evaporator. The Zr content of the precursor solution was varied as an additional mole fraction relative to the Y content in the range 1–20 mol% (i.e., ∼0.4–8 vol% or wt%). The resulting organometallic source vapor was then transported by argon and mixed with oxygen before being sprayed through a custom-designed showerhead onto the heated substrate. All the Zr-modified YBCO samples, about 0.9 μm thick, were processed in a reel-to-reel configuration, under an oxygen partial pressure of 0.5 Torr at a total system pressure of 2.5 Torr. During the depositions, the heater temperature was maintained near 950 °C based on prior process optimization for high quality REBCO growth [11]. This procedure enabled the study of variations/trends in structural properties and superconducting performance of YBCO films with respect to Zr content. The LMO/IBAD-MgO templates used in this study were fabricated using pilot scale equipment at SuperPower, Inc. [12]. The phase and crystallographic orientation of the Zr-modified films were investigated by x-ray diffraction (XRD). The surface morphology and cross-sectional microstructure examinations were made using a JEOL Model JSM-840 scanning electron microscope (SEM) and a Hitachi HF-3300 transmission electron microscope (TEM) operating at 300 kV. Transport measurements of superconducting critical temperature T_c, and J_c were conducted using a standard four-probe technique along the tape axis. The width of each sample was 12 mm. Values for J_c were assigned at a 1 μV cm^{-1} criterion. The imaging Raman microscopy was performed using a Renishaw InVia Raman System.

Coordinated Raman micro-spectroscopy, x-ray near-edge spectroscopy (XANES), and extended x-ray absorption fine structure (EXAFS) analyses were also made on the Zr-modified samples. Details of the measurement techniques and the results obtained are reported in the accompanying article of this issue [13].

3. Results and discussion

In our previous work, we found that the deposition rate plays a crucial role in obtaining columnar structures of BZO within the MOCVD-based REBCO films [9]. Note that the self-assembly likely occurs due to strain minimization. Such a process is expected to be dependent on the deposition rate for complete phase separation and effective, long-range self-assembly [14]. Hence, as reported in [9], self-assembly of BZO nanodots into columnar defects was achieved by reducing the deposition rate (R_{dep}) from 0.5 to 0.13 μm min^{-1} during the growth of MOCVD films. In accordance with this observation, we first evaluated the performance of our research set up with respect to systematic variations in R_{dep} (0.06–0.2 μm min^{-1}). Starting with a Zr composition of 5 mol%, the influences of both Zr additions and the R_{dep} on the transport properties of YBCO films are shown in figures 1(a) and (b). For comparison, typical data for a standard MOCVD-YBCO film (processed at R_{dep} = 0.2 μm) with no Zr addition are also shown. Two important effects can be deduced from these figures:

(i) Zr additions significantly improve the pinning performance of MOCVD-YBCO, in that both the magnetic field

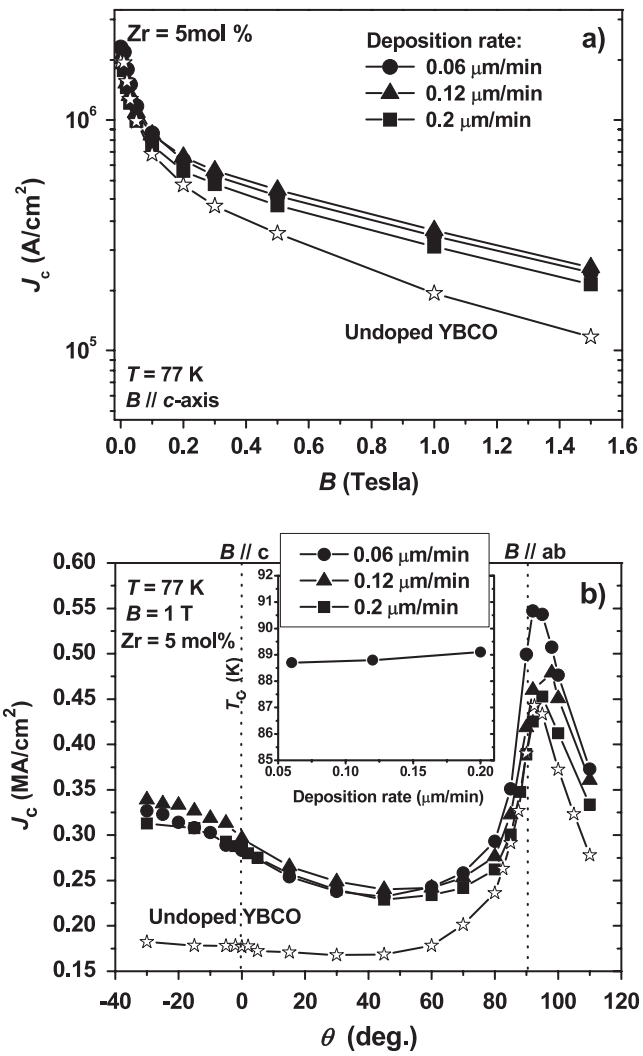

Figure 1. Plotted in (a) and (b) are the magnetic field and angular dependent transport J_c at 77 K for 5 mol% Zr-added MOCVD-YBCO films at various deposition rates (R_{dep}), respectively. The inset of (b) shows the variation in T_c as a function of R_{dep}.

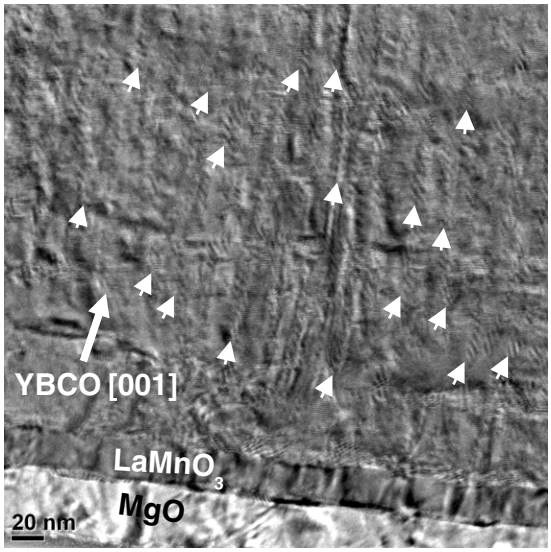

Figure 2. Cross-section high-resolution TEM image of 5 mol% Zr-modified YBCO film deposited at $R_{dep} = 0.2\ \mu m\ min^{-1}$, showing the columnar defects (some of them indicated by small arrows) responsible to the enhanced pinning for field orientations close to the *c*-axis.

(figure 1(a)) and the angular dependence (figure 1(b)) of J_c are enhanced. In particular there is noticeably a broad peak for field orientations near the *c*-axis ($\theta = 0°$), suggesting the presence of additional correlated defects aligned approximately near the surface normal of the YBCO film. In fact, for the specimen processed at $R_{dep} = 0.2\ \mu m\ min^{-1}$, figure 2 shows numerous *c*-axis aligned columnar structures, with 'splayed' appearance, comprised of self-assembled nano-sized BZO platelets. It is noteworthy that the J_c peak when the field is parallel to the *ab*-planes is somewhat shifted in angle; this is due to the ion beam assisted deposition of the buffer layers, which results in a slight tilt away from the surface normal. The flux pinning associated with the extended defects is also tilted away from the *c*-axis. As a result, the angular range between this peak and the *ab*-peak is less than 90° in one quadrant and greater than 90° in the other quadrant. Only one quadrant is shown in figure 1(b). Even though the MOCVD process is quite different from the PLD process, the microstructure shown in figure 1(c) closely resembles that obtained in BZO-doped PLD YBCO films [5–7]. Note that, while a reaction between the added Zr and Ba (from the YBCO) takes place to form BZO during the MOCVD process, a target doped with pre-formed nanoparticles of BZO is generally used for the PLD processes.

(ii) It is also observed that the deposition rate does not strongly affect the pinning or superconducting performance of Zr-added films, provided that $R_{dep} \leqslant 0.2\ \mu m\ min^{-1}$. Notice also the similarity in T_c values with respect to R_{dep} from the inset of figure 1(b).

After having established these proof-of-principal results on 5 mol% Zr-modified composition, the effects of varying the mole percentage of Zr-added on the performance of the MOCVD-YBCO films were investigated. For consistency, all the results presented hereafter were obtained on samples (YBCO thickness ~0.9 μm) processed with the highest deposition rate of 0.2 μm /min. The crystal structure and phase development of BZO for all Zr-added samples were analyzed with XRD. Figure 3(a) shows a series of θ–2θ diffraction patterns in the vicinity of the YBCO (103) reflection for films modified with 1–20 mol% Zr additions. In order to prevent interference with MgO from the substrate, scans are made through the BZO (101) reflection, since MgO (101) reflections are not allowed. For all Zr compositions, the BZO nanoparticles are crystalline and grow heteroepitaxially with the YBCO, and as expected the magnitude of the (101) peak becomes stronger with increasing dopant level. Using the Scherrer formula [15], an average BZO crystallite size of ~7.5 nm was calculated from the widths of the (101) diffraction lines, with a tendency of a slight increase to ~8.8 nm as the Zr content increases from 2.5 to 20 mol%

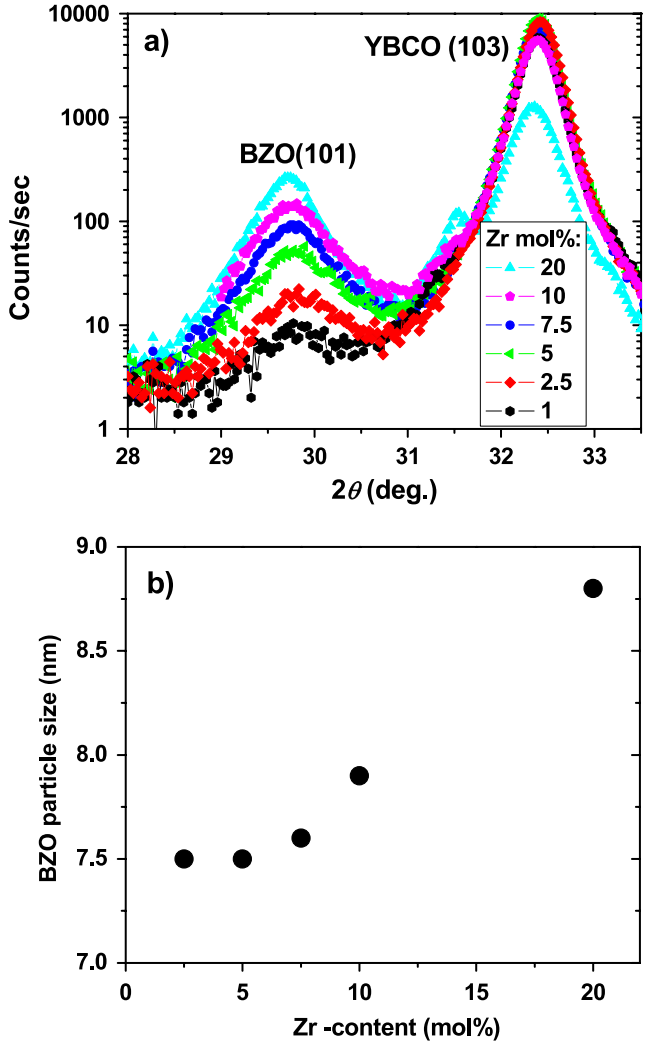

Figure 3. (a) A series of XRD scans taken at the vicinity of the YBCO (103) reflection, showing evolution of the BZO phase for MOCVD-YBCO films doped with various mole percentages of Zr; (b) the BZO crystallite size as a function of Zr doping level, inferred from the Scherrer formula.

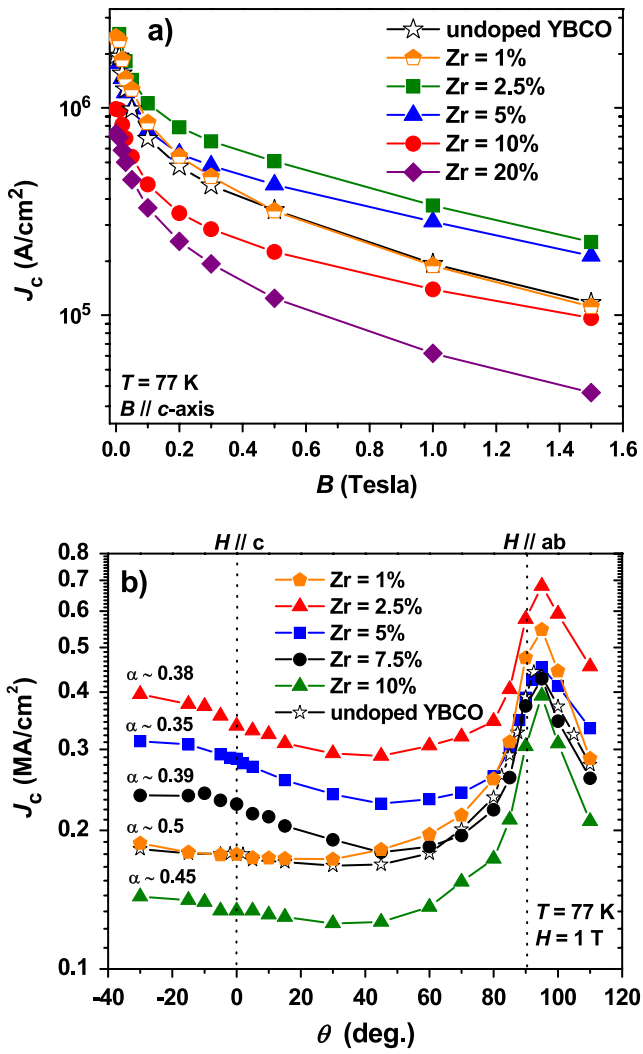

Figure 4. Plot of (a) the magnetic field dependence of transport J_c ($B \parallel c$-axis) at 77K for 0.9 μm-thick MOCVD-YBCO films containing various amounts of added Zr; (b) the dependence of J_c, for the same samples presented in part (a), on the orientation of the field angle relative to the c-axis direction, measured in a 1 T applied field (maximum Lorentz force configuration).

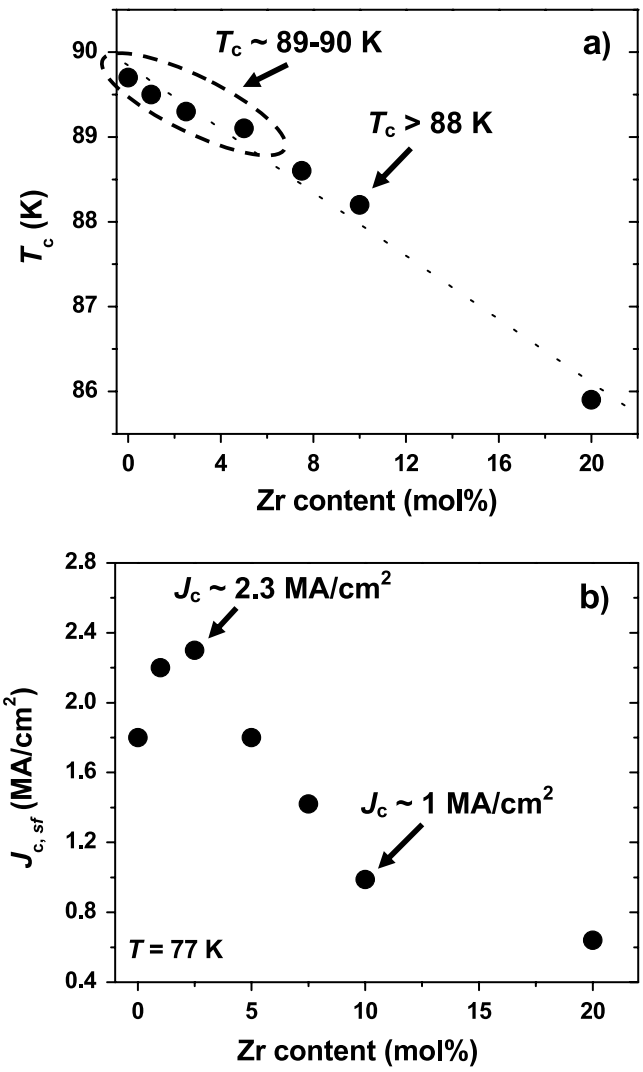

Figure 5. Dependence of (a) T_c and (b) self-field J_c (77 K) on the various levels of Zr mol% for 0.9 μm-thick MOCVD-YBCO films.

(figure 3(b)). The 'crystallite size' is presumably $\sim$ the diameter of the nanocolumn, since the BZO particles stack coherently along the c-direction. This result is consistent with the TEM observation shown in figure 2, and implies that the Zr content in this range does not strongly influence the BZO size. A low-angle shoulder appears on the YBCO (103) peak at 20 mol% Zr, indicating either the appearance of a third phase or structural changes to the YBCO phase. In addition, the decrease in the XRD peak intensity at this dopant level is related to a significant reduction in YBCO volume fraction from $\sim$94% (for 2.5 mol% Zr) to $\sim$74% (20 mol% Zr) as deduced from the peak widths.

Next, we turn to the effect of Zr content on the in-field performance of YBCO films. Figure 4(a) shows the magnetic field dependence of transport J_c for $B \parallel c$ at 77 K for a typical undoped MOCVD-YBCO film (for comparison) and for films modified with 1–20 mol% Zr additions. While little improvement occurs for 1 mol% Zr addition, an enhanced J_c performance is observed for other compositions <10 mol%. In particular, the sample modified with 2.5 mol% Zr addition exhibits the largest improvement in J_c, showing a factor-of-two enhancement over the undoped film at 1 T. These Zr-modified films also had higher self-field (sf) J_c values of 2.2–2.4 MA cm^{-2} (versus J_c (sf, 77 K) $\sim$1.8 MA cm^{-2} for undoped YBCO). On the other hand, net degradation sets in at doping levels above 7.5 mol%. Similar trends were observed in the angular dependent J_c measurements (figure 4(b)) at $B =$ 1 T. Also, for doping levels up to 10 mol% the broad peak about the c-axis is consistent with the attainment of a smaller power-law exponent $\alpha \sim 0.35$–0.39 in the low-field regime ($\sim$0.1–1 T at 77 K), where $J_c \propto B^{-\alpha}$. For the undoped YBCO film, the α value of about 0.5 is typical for MOCVD-based REBCO films, where a peak is generally absent for orientations about the c-axis [16, 17]. Accordingly, the absence of a c-axis peak for the 1 mol% composition suggests that too low a level of added Zr is not conducive to the formation of a columnar array, although some BZO has formed according to figure 3(a). Rather, it is likely that the BZO formed/distributed as individual particles

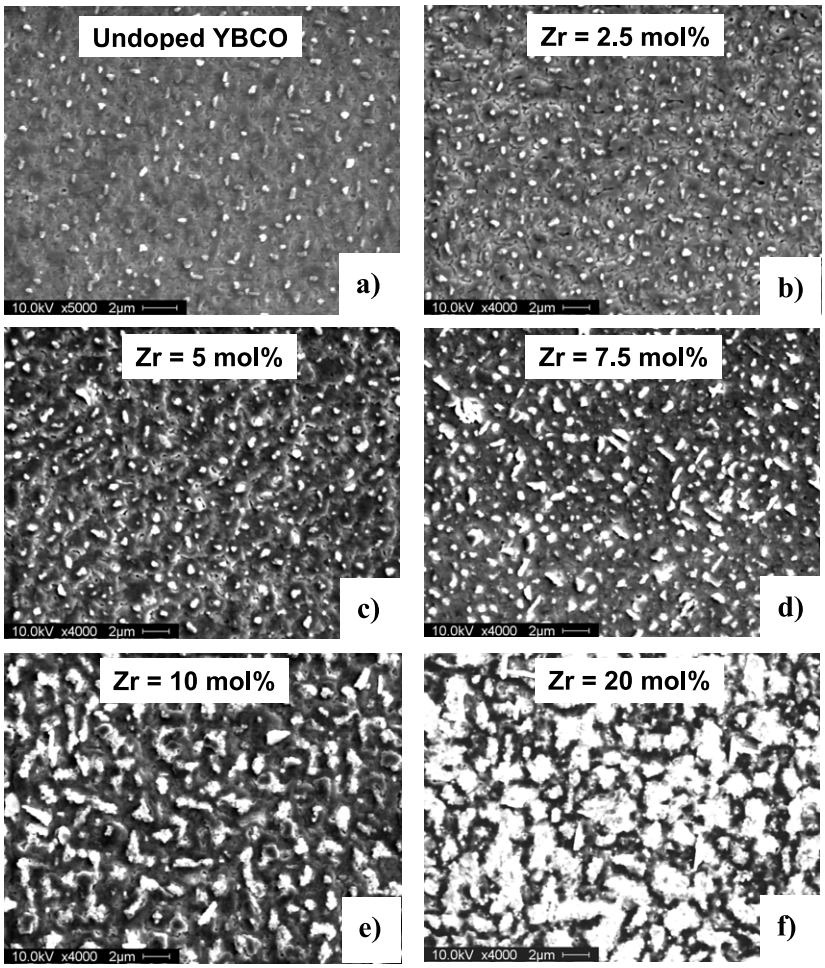

Figure 6. Plan view SEM surface morphologies for MOCVD-YBCO films deposited on IBAD-MgO templates with and without Zr-additions. (a) Undoped, 0 mol%, (b) 2.5 mol%, (c) 5 mol%, (d) 7.5 mol%, (e) 10 mol%, (f) 20 mol%.

throughout the YBCO matrix, which indeed provides a small enhancement of J_c at fields below ∼0.5 T. Based on these results, it appears that the most effective pinning occurs for doping levels in the range of 2.5–5 mol%. As the doping level increases, especially above 7.5 mol%, the strength of the *c*-axis pinning decreases accompanied by deterioration of the superconducting properties of the samples. Further evidence for this is presented in figures 5(a) and (b), showing the variations in T_c and self-field J_c, respectively, as a function of the nominal Zr concentration. While T_c shows a slow linear decrease, with values remaining above 88 K up to the 10 mol% level, the J_c (sf, 77 K) values exhibit first an improvement for additions up to 2.5 mol% (∼2.3 MA/cm^2), followed by a sharp decrease with a further increase in the Zr content ($J_c \sim 1$ MA/cm^2 for 10 mol%). Similar trends in T_c and J_c have also been reported for laser-ablated BZO-doped YBCO films [18–20]. However, in those PLD studies, the reduction in T_c with respect to BZO concentration is found to be far more prominent than in the present case. Although both techniques involve layer-by-layer *in situ* film growth, the nominal deposition temperature for our MOCVD films is somewhat higher. In [17] the decrease in T_c is attributed to the increased strain in YBCO with incorporation of BZO nanoparticles. This would most likely require strain fields due to the BZO columns to overlap or extend within a coherence length; otherwise high-T_c percolative paths would exist. In the present case, we ascribe the decrease in T_c primarily to the formation of increased secondary phase segregates, i.e., CuO, along with increased global cation disorder in the YBCO lattice, the details of which will be discussed below.

Regarding the result in figure 5(b), an observation of interest is that a maximum in J_c with respect to doping level has been realized previously for BZO-doped YBCO by PLD [21]. In the present case, the gradual fall-off of T_c with Zr concentration in figure 5(a) serves to suppress the pinning energy, although the 1–2% decrease in T_c from a 2.5 mol% to 10 mol% level cannot account for the ∼50% drop in J_c (sf), especially considering that the XRD pole figure analysis reveals very little change in YBCO texture with Zr concentration. In [21], however, it was shown that, for conditions where BZO content increases only the BZO column diameter, a maximum in J_c versus doping concentration can be expected. The phenomenon arises due to a competition between an increase in columnar defect pinning energy with BZO crystallite diameter [22], and a decrease due to the effect of increasing the global penetration depth [23]. The description

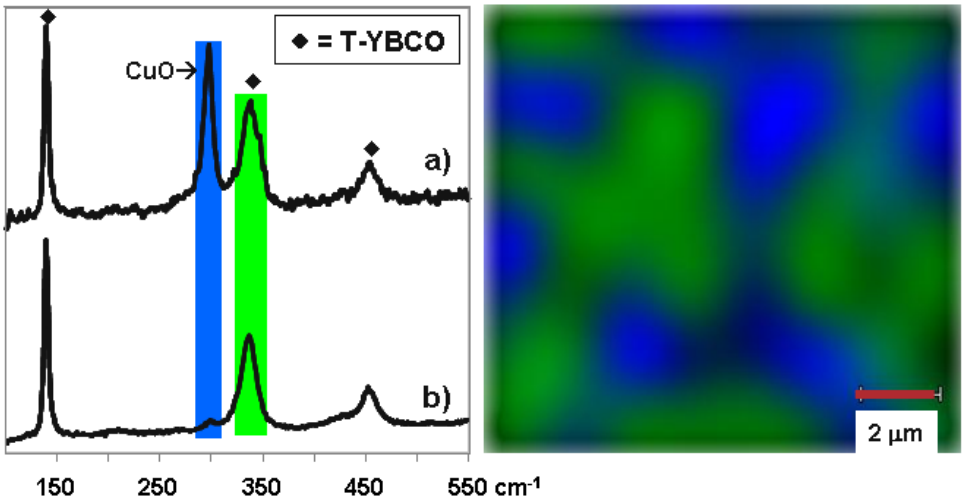

Figure 7. The right panel shows a Raman image of a 10 μm × 10 μm area on the surface of the 20 mol% Zr film (an area comparable to that shown in figure 6(f)). Spectrum (a) in the left panel is from the set of scans that was used to create the image. Spectrum (b) is the top surface spectrum of the 2.5 mol% film (shown for comparison of relative CuO content).

of the latter effect, developed in [23], is somewhat subtle but describes how an array of non-superconducting columns effectively changes the overall free energy of the system, with the ramification of an decrease in the vortex line energy and increase in the effective penetration depth. As in [21], here we employed a somewhat modified analysis yielding a qualitatively peaked J_c with Zr content—an issue that will be pursued in more detail in a subsequent publication.

To place these results in perspective with the material properties, SEM and Raman microscopy studies were conducted on samples with and without Zr modifications. It is apparent from the SEM images (figures 6(a)–(f)) that as the Zr mol% increases, the microstructure of the YBCO films is modified, as evidenced by the increased secondary phases, mainly Cu–O on the surface, which become much more prominent beyond 7.5 mol% Zr additions. The proliferation of these secondary phases could affect the grain connectivity and hence current percolation, thereby degrading the J_c performance of these films significantly. In fact, at higher Zr levels, especially $\geqslant$10 mol%, TEM analysis indicated that some secondary phases nucleate close to the YBCO/buffer interface and extend over a thickness comparable to the entire YBCO thickness.

The phase composition on the surface of the 20 mol% film shown in figure 6(f) was examined by imaging Raman microscopy. A 10 μm × 10 μm area was imaged with 633 nm excitation focused to a ca. 1 μm diameter spot. The image, shown in the right panel of figure 7, was created from 121 spectra taken in 1 μm increments using a snake motion pattern. (Spectrum 'a' in the left panel of figure 7 is typical of the spectra in this set.) Blue identifies the CuO dominant areas imaged using the 300 cm^{-1} CuO phonon. Green identifies the YBCO dominant areas imaged using the 330 cm^{-1} YBCO phonon. The size of the imaged area is much the same as that in figure 6(f). Spectrum 'b' in the left panel of figure 7 is from the top surface of the 2.5 mol% film and is included to provide a comparison of the relative surface CuO increase with increasing Zr from 2.5 to 20 mol%.

More extensive information on through-thickness sample-to-sample variations, of phase chemistry and microstructure were obtained from additional Raman microprobe measurements. These detailed analyses by Raman micro-spectroscopy are the focus of the accompanying paper [13]. Here we briefly mention that the Raman results revealed considerably more lattice atom disorder in YBCO films beyond 7.5 mol% Zr-added. This observation may be related to the fact that increased Zr will sequester more Ba (since BZO forms through reaction with available Ba), leaving less available Ba in the film matrix.

4. Summary

In summary, the efficacy of pinning enhancements in MOCVD-YBCO films through Zr additions has been investigated on LMO/IBAD-MgO templates. Emphasis has been placed on the systematic variations in structural and superconducting properties with respect to varying mole percentages of added Zr. Some highlights of the present study are as follows: (i) Zr additions improve the in-field J_c performance of MOCVD-YBCO films due to the formation of *c*-axis aligned BZO-based columnar defects; (ii) optimum performance is obtained with doping levels around 2.5–5 mol%; (iii) above these levels, YBCO performance decreases considerably, due we believe to a combination of factors that includes increase in BZO particle size, slightly decrease in T_c; at higher Zr levels increase in secondary phases (mainly CuO) and cation disorder. The results presented in this work establish a basis for flux pinning in MOCVD-YBCO films with Zr additions. These results also emphasize the complementary and supplemental role of different characterization techniques in detailed evaluation of the samples.

Acknowledgment

This work was done as part of the ORNL-SuperPower and the ANL-SuperPower CRADA and supported by the US

Department of Energy, Office of Electricity Delivery and Energy Reliability. The research was performed at the Oak Ridge National Laboratory, managed by U.T.-Battelle, LLC for the USDOE under contract no. DE-AC05-00OR22725, and at Argonne National Laboratory under contract no. DEAC02-06CH11357 between UChicago Argonne, LLC and the USDOE. The imaging Raman microscopy was performed at the Argonne National Laboratory Center for Nanoscale Materials.

References

[1] Larbalestier D, Gurevich A, Feldman D M and Polyanski A 2001 High-T_c superconducting materials for electric power applications *Nature* **414** 368

[2] Paranthaman M P and Izumi T 2004 High performance YBCO coated superconducting wires *MRS Bull.* **29** 8 (special issue)
Paranthaman M P and Selvamanickam V 2007 *Flux Pinning and AC Loss Studies on YBCO Coated Conductors* (New York: Nova Science)

[3] Foltyn S R, Civale L, MacManus-Driscoll J L, Jia Q X, Maiorov B, Wang H and Maley M 2007 Materials science challenges for high-temperature superconducting wire *Nat. Mater.* **6** 631

[4] MacManus-Driscoll J L, Foltyn S R, Jia Q X, Wang H, Serquis A, Civale L, Maiorov B, Hawley M E, Maley M P and Peterson D E 2004 Strongly enhanced current densities in superconducting coated conductors of $YBa_2Cu_3O_{7-\delta} + BaZrO_3$ *Nat. Mater.* **3** 439

[5] Goyal A *et al* 2005 Irradiation-free, columnar defects comprised of self-assembled nanodots and nanorods resulting in strongly enhanced flux-pinning in $YBa_2Cu_3O_{7-\delta}$ films *Supercond. Sci. Technol.* **18** 1533

[6] Kang S *et al* 2006 High-performance high-T_c superconducting wires *Science* **311** 1911

[7] Wee S H, Goyal A, Zuev Y L and Cantoni C 2008 High performance superconducting wire in high applied magnetic fields via nanoscale defect engineering *Supercond. Sci. Technol.* **21** 1

[8] Yamada Y *et al* 2005 Epitaxial nanostructure and defects effective for pinning in $Y(RE)Ba_2Cu_3O_{7-\delta}$ coated conductors *Appl. Phys. Lett.* **87** 132502

[9] Chen Y, Selvamanickam V, Zhang Y, Zuev Y, Cantoni C, Specht E, Parans Paranthaman M, Aytug T, Goyal A and Lee D 2009 Enhanced flux pinning by $BaZrO_3$ and $(Gd, Y)_2O_3$ nanostructures in metal organic chemical vapor deposited GdYBCO high temperature superconductor tapes *Appl. Phys. Lett.* **94** 062513

[10] Selvamanickam V *et al* 2001 High-current Y-Ba-Cu-O coated conductor using metal organic chemical-vapor deposition and ion-beam-assisted deposition *IEEE Trans. Appl. Supercond.* **11** 3379

[11] Aytug T, Paranthaman M, Heatherly L, Zuev Y, Zhang Y, Kim K, Goyal A, Maroni V A, Chen Y and Selvamanickam V 2009 Deposition studies and coordinated characterization of MOCVD YBCO films on IBAD-MgO templates *Supercond. Sci. Technol.* **22** 1

[12] Xiong X M, Lenseth K P, Reeves J L, Rar A, Qiao Y F, Schmidt R M, Chen Y M, Li Y J, Xie Y Y and Selvamanickam V 2007 High throughput processing of long-length IBAD MgO and epi-buffer templates at SuperPower *IEEE Trans. Appl. Supercond.* **17** 3375

[13] Maroni V A *et al* 2010 Raman and x-ray absorption spectroscopy characterization of Zr-doped MOCVD $YBa_2Cu_3O_{6+\delta}$ *Supercond. Sci. Technol.* **23** 014020

[14] Goyal A 2007 Engineered columnar defects for coated conductors *Presented at the 2007 Annual Peer Review of the US Superconductivity Program for Electric Systems* http://www.energetics.com/supercon07

[15] Cullity B D and Stock S R 2001 *Elements of X-ray Diffraction* (Upper Saddle River, NJ: Prentice-Hall)

[16] Chen Y *et al* 2008 Recent progress in second-generation HTS wire technology at SuperPower *Mater. Res. Soc. Symp. Proc.* **1099E** 1099-II01-02

[17] Selvamanickam V *et al* 2009 High performance 2G wires: from R&D to pilotscale manufacturing *IEEE Trans. Appl. Supercond.* at press

[18] Kang S, Goyal A, Li J, Martin P, Ijaduola A, Thompson J R and Paranthaman M 2007 Flux-pinning characteristics as a function of density of columnar defects comprised of self-assembled nanodots and nanorods in epitaxial $YBa_2Cu_3O_{7-\delta}$ films for coated conductor applications *Physica* C **457** 41

[19] Peurla M, Paturi P, Stepanov Y P, Huhtinen H, Tse Y Y, B'odi A C, Raittila J and Laiho R 2006 Optimization of the $BaZrO_3$ concentration in YBCO films prepared by pulsed laser deposition *Supercond. Sci. Technol.* **19** 767

[20] Ichinose A, Naoe K, Horide T, Matsumoto K, Kita R, Mukaida M, Yoshida Y and Horii S 2007 Microstructures and critical current densities of YBCO films containing structure-controlled $BaZrO_3$ nanorods *Supercond. Sci. Technol.* **20** 1144

[21] Goyal A, Christen D K and Paranthaman M 2006 Epitaxial coatings for coated conductors *Presented at the 2006 Annual Peer Review of the US Superconductivity Program for Electric Systems* http://www.energetics.com/meetings/supercon06/pdfs/Strategic%20Research/Wednesday/04_Strategic_Research_ORNL_Paranthaman.pdf

[22] Nelson D R and Vinokur V M 1993 Boson localization and correlated pinning of superconducting vortex arrays *Phys. Rev.* B **48** 13060

[23] Wahl A, Hardy V, Provost J, Simon Ch and Buzdin A 1995 Unusual field dependence of the reversible magnetization in heavy ions irradiated thallium-based single crystals *Physica* C **250** 163